https://doi.org/10.5194/ar-2023-21
Preprint. Discussion started: 4 January 2024

AEROSOL Research Discussions

A multi-instrumental approach for calibrating two real-time mass spectrometers using high performance liquid chromatography and positive matrix factorization

Melinda K. Schueneman[1], Douglas A. Day[1], Dongwook Kim[1], Pedro Campuzano-Jost[1], Seonsik Yun[1], Marla P. DeVault[1], Anna C. Ziola[1], Paul J. Ziemann[1], and Jose L. Jimenez[1]

[1]Department of Chemistry and Cooperative Institute for Research in Environmental Sciences, University of Colorado, Boulder, CO 80309, USA

Corresponding Author: Jose Jimenez, jose.jimenez@colorado.edu

Abstract. Obtaining quantitative information from real-time soft-ionization aerosol instruments such as an Extractive Electrospray time-of-flight Mass Spectrometer (EESI) can be challenging, due to many individual species having different, and often hard to predict, sensitivities. Directly calibrating is time-consuming and relevant standards are often hard to obtain. In addition, the molecular identities of many of the sampled species may be ambiguous. Bulk OA sensitivities are sometimes used to estimate molecular sensitivities, but different types of OA can have bulk sensitivities that vary by a factor of ~10. A system to separate the compounds present in complex samples can enable their direct calibration. Here, high performance liquid chromatography (HPLC) followed by aerosol formation via atomization was combined with online, 1 Hz measurements to calibrate the EESI and a High Resolution Aerosol Mass Spectrometer (AMS) for compounds present in a secondary organic aerosol (SOA) mixture. Pure compounds were used to test the method and characterize its uncertainties. Pure compound calibration factors were consistent within ±20% for direct atomization vs. HPLC separation, which is far superior to the orders of magnitude sensitivity differences that are possible with EESI. For species that were not well separated by chromatography, Positive Matrix Factorization (PMF) based on AMS spectra was used to test its ability to separate overlapping species. In two test cases, further separation was achieved using PMF, but derived sensitivities from direct and HPLC calibrations varied by up to a factor of 2.

https://doi.org/10.5194/ar-2023-21
Preprint. Discussion started: 4 January 2024

AEROSOL Research Discussions

26 **TOC figure**

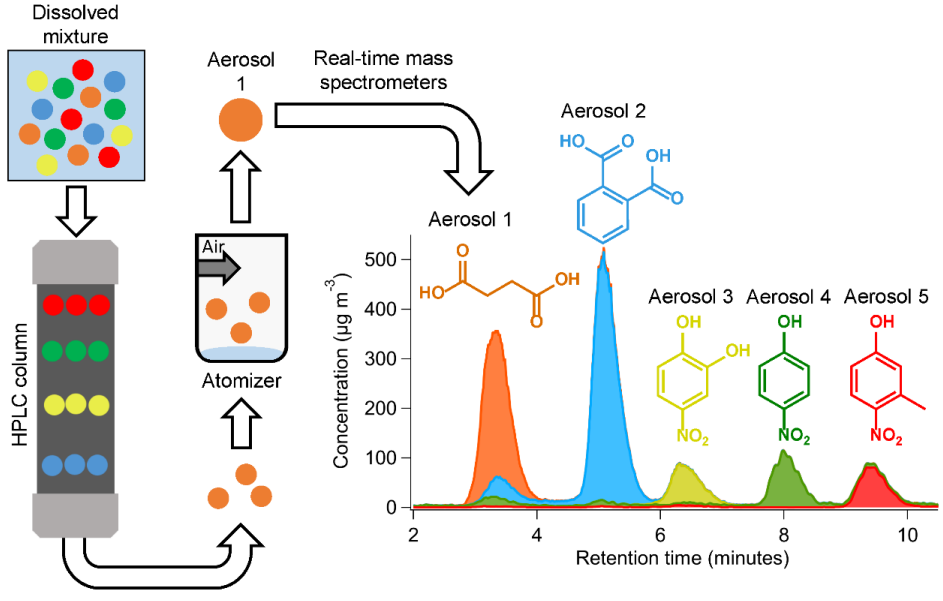

27

https://doi.org/10.5194/ar-2023-21
Preprint. Discussion started: 4 January 2024

AEROSOL Research Discussions

1 Introduction

Atmospheric aerosols are a complex, and often poorly understood, component of Earth's atmosphere. Aerosols have significant effects on both human and ecosystem health, and are significant contributors to anthropogenic climate forcing (Dockery et al., 1996; Lighty et al., 2000; Lohmann et al., 2004; IPCC, 2013). Organic aerosol (OA) is a substantial component of global aerosol levels (Kanakidou et al., 2005; Zhang et al., 2007; Jimenez et al., 2009). Since the early 2000s an important instrument for measuring OA concentrations in real-time has been the Aerosol Mass Spectrometer (AMS) (Jayne et al., 2000; Canagaratna et al., 2007) and its high-resolution version (HR-AMS) (DeCarlo et al., 2006). Soft-ionization aerosol mass spectrometers, such as the Extractive Electrospray Time-of-Flight Mass Spectrometer (EESI-ToF-MS, EESI hereinafter), have more recently become important tools for obtaining more detailed OA speciation (Lopez-Hilfiker et al., 2014, 2019; Eichler et al., 2015).

EESI can detect individual molecular ions (referred to henceforth as either molecular ions or individual species, even if they may comprise several isomers) from the particle-phase with 1 s time resolution (Lopez-Hilfiker et al., 2019; Pagonis et al., 2021). EESI has been used to measure aerosols in urban areas (Qi et al., 2019, 2020; Stefenelli et al., 2019; Kumar et al., 2022), in biomass burning (Qi et al., 2019; Pagonis et al., 2021), in cooking emissions (Qi et al., 2019; Brown et al., 2021), and for chamber studies of secondary OA (SOA) formation (Liu et al., 2019; Pospisilova et al., 2020). Many studies have illustrated the low detection limits, limited fragmentation, and other capabilities of the EESI; e.g. Lopez-Hilfiker et. al. (2019) and Pagonis et. al. (2021).

However, obtaining quantitative information for individual species from EESI measurements of complex mixtures of unknown species can be challenging, due to each species having different, and often hard to predict, sensitivities (Law et al., 2010; Lopez-Hilfiker et al., 2019; Brown et al., 2021; Wang et al., 2021). In addition, EESI measures molecular ions, but can in some cases cause fragmentation, such as due to loss of HNO_3 from nitrates (Liu et al., 2019). For an SOA mixture from a single precursor, the bulk sensitivity compared to SOA formed from a different precursor has been shown to vary by a factor of 15 or more (Lopez-Hilfiker et al., 2019). Different studies also show that the bulk sensitivity for OA formed from different emission sources (e.g. cooking, biomass burning) can vary by a factor of ~10 (Qi et al., 2019; Stefenelli et al., 2019; Brown et al., 2021). For pure organic standards, the sensitivity can vary by a factor of 30 or more (Lopez-Hilfiker et al., 2019). Instead of directly measuring compound sensitivity, some groups use machine-learning (Liigand et al., 2020) or thermodynamic modeling (Kruve et al., 2014) to approximate instrument response factors for individual species. Other studies use bulk calibration factors for complex mixtures as an approximation for quantification (Tong et al., 2022).

Sensitivities can vary due to differences in analyte solubility (Law et al., 2010), EESI working fluid composition, sample composition, and different instrument conditions and settings, including polarity and changes in inlet pressure (Lopez-Hilfiker et al., 2019; Pagonis et al., 2021). Calibrating the EESI for individual species can be a challenging task, especially when standards are unavailable for most atmospheric oxidation products. In addition, OA from chamber experiments or field studies often contains unidentified molecular ions, or those whose species identity is ambiguous.

Several calibration methods have been applied to EESI. For example, direct calibrations were performed for many organic standards in Lopez-Hilfiker et. al. (2019), for 4-nitrocatechol (EESI(-)) and levoglucosan (EESI+)

https://doi.org/10.5194/ar-2023-21
Preprint. Discussion started: 4 January 2024

in Pagonis et al. (2021) to track sensitivity during each aircraft flight, and levoglucosan for regular sensitivity tracking during an indoor cooking study (and several other compounds less frequently and bracketing the campaign) in Brown et. al. (2021). During research field studies, often only one or two species are calibrated frequently, and the rest are quantified using relative response factors measured less frequently (Qi et al., 2019; Brown et al., 2021; Pagonis et al., 2021).

A recent paper combined measurements from the Vocus Proton-Transfer Mass Spectrometer (Vocus), AMS, and EESI to measure speciated response factors without the need for standards. In that study, SOA was generated using an Oxidation Flow Reactor (OFR). Following SOA formation, the Vocus measured the gas phase species, and the AMS and EESI measured the bulk and speciated particulate phase, respectively. EESI response factors were obtained through comparison to decreasing gas-phase mixing ratios measured by the Vocus as they condensed to the particle-phase (Wang et al., 2021).

Another method for obtaining calibration information is Positive Matrix Factorization (PMF). PMF is a type of factor analysis that allows approximately apportioning aerosol mass measured with online mass spectrometer and other instruments to atmospheric sources or level of oxidation (Zhang et al., 2005; Lanz et al., 2007; Ulbrich et al., 2009). To our knowledge, PMF has not been used with AMS data alone to obtain mass spectra and time series for individual molecular components. Separation with PMF alone would be difficult for ambient or chamber experiment data, in part, since most compounds likely co-vary in time and thus would not be statistically resolvable (Craven et al., 2012). Direct calibrations have been conducted to generate high-resolution AMS mass spectra for individual species (Ulbrich et al., 2019). A combination of AMS and PMF has been used to obtain quantitative information for EESI bulk measurements or PMF factors (Qi et al., 2019, 2020; Kumar et al., 2022). PMF has also been used on a combined data set consisting of both EESI and AMS data (Tong et al., 2022).

To our knowledge, PMF has not been applied previously to AMS and EESI chromatographically-separated data. Running PMF on chromatographic data may be able to generate species-specific mass spectra for compounds that cannot be obtained directly. PMF has been applied in the past to GC-MS data (Zhang et al., 2014, 2016; Gao et al., 2018), but not to High Performance Liquid Chromatography (HPLC) data, which is better suited for oxidized SOA species than GC, to our knowledge. AMS detection following HPLC separation has been conducted previously (Farmer et al., 2010) to explore AMS spectra of the separate compounds, but not for quantification. HPLC has not been previously combined with EESI or PMF, to our knowledge.

Here, for the first time, we demonstrate a method combining High Performance Liquid Chromatography (HPLC), atomization, and detection by EESI, AMS, and Scanning Mobility Particle Sizer (SMPS). The method was validated by separating a mixture of standards, and then applied to chamber SOA. The analyte peak measured with each instrument was integrated, and calibration factors for separated species were calculated for the EESI. The AMS response factor (CF_x^A, or RIE*CE, the product of the relative ionization efficiency and collection efficiency) and the atomic oxygen to carbon (O:C) ratio for different analytes were quantified. EESI calibration factors (CF_x^E) for individual compounds were determined and compared to literature values. In cases where full peak separation via HPLC alone was not achieved, PMF was run on the EESI and AMS mass spectral matrices to obtain further compound separation.

https://doi.org/10.5194/ar-2023-21
Preprint. Discussion started: 4 January 2024

2 Methods

2.1 Chamber experiments and filter mass collection

SOA was generated using the procedure of DeVault et. al. (2022). Briefly, chamber experiments were conducted in a 6.9 (±0.5) m^3 teflon chamber (Bakker-Arkema and Ziemann, 2021). The temperature (23°C) and atmospheric pressure (0.83 atm) were constant. Ammonium sulfate seed was added to a humidified chamber (RH=55%), followed by β-pinene, which was evaporated from a heated glass bulb. In the dark, N_2O_5 was added as the NO_3 source, from the sublimation of cryogenically-trapped solid N_2O_5. The experiment was modeled after Claflin et. al. (2018).

Following SOA formation, a 0.45 μm Millipore Fluoropore PTFE filter was used to collect SOA. The filter+aerosol was weighed after aerosol collection. The filter+aerosol was exposed to minimal ambient air, and was always handled with artificial lighting turned off and outdoor blinds drawn. After weighing, each filter was extracted in 2 mL of HPLC grade ethyl acetate (EtAc) twice. The 4 mL aerosol extract/EtAc mixture was dried using pure N_2. Once the EtAc was evaporated, the leftover material was dissolved in HPLC grade acetonitrile (ACN) and stored in a freezer at -23°C (DeVault et al., 2022). The extract used here was the same as DeVault et. al. (2022), and was one year old at the time of analysis. That study showed that the SOA is composed entirely of acetal dimers, which are exceptionally stable, so the SOA is unlikely to have changed over this period.

2.2 High Performance Liquid Chromatography (HPLC)

HPLC separation was performed using a Shimadzu Prominence HPLC, coupled to a Zorbax Eclipse XDB-C18 column (250 × 4.6 mm with 5 μm particle size). A Nexera X2 SPDM30A UV/vis photodiode array detector was used to generate absorbance chromatograms. The column stationary phase was designed for reverse mode, where smaller, more polar species had shorter elution times. Separated species were measured first at **λ**=210 and **λ**=254 nm using an UV-Vis diode array detector with a reference wavelength of 300 nm. Separated chemical components then flowed into a high-flow Collison atomizer, forming droplets and then aerosols consisting solely of the SOA compounds after evaporating the HPLC solvent in a Nafion drier. The aerosols were then measured by a suite of instruments, shown in Fig. 1, and pictured in Fig. S1. Tubing delay times are also included in Table S1.

https://doi.org/10.5194/ar-2023-21
Preprint. Discussion started: 4 January 2024

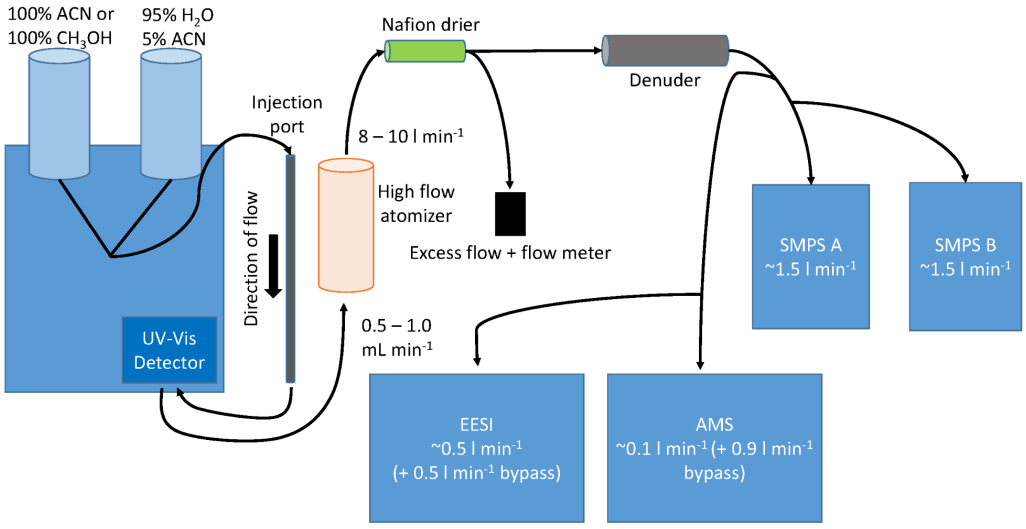

Figure 1. HPLC schematic. Left, HPLC containing a column and a UV-Vis detector. Following separation, the column effluent was sent to an atomizer, dried, and the aerosol was detected by each of the instruments shown.

A maximum volume of 50 µL ACN/aerosol mixture was injected into the column at once. At the beginning of each day, the HPLC solvent lines (HPLC grade acetonitrile and HPLC grade water) were flushed to remove any air bubbles that may affect elution. Following this, a clean cycle was run by injecting 50 µL HPLC grade ACN into the reverse-phase column. This ensured previous HPLC run species did not contaminate new runs. The first run of the day, post cleaning cycle, was a 4-nitrocatechol/4-nitrophenol mixture (dissolved in ACN). These species were well characterized by the particle-phase instruments and have measurable absorbances at the recorded UV wavelengths.

For each experiment, the mobile phase consisted either of an ACN/water mixture or an ACN/CH_3OH/water mixture. The mixture varied in relative concentrations of each solvent over the course of each HPLC run. Most experiments were started at 95% water/5% ACN (solvent mixture A). The mobile phase became less polar over time. For some systems, solvent B (pure acetonitrile) replaced solvent system A as time went on. For other systems, solvent C (pure methanol) was used. Each standard and/or SOA system was run under different conditions, depending on the separability of different components.

For the standard solution run, a mixture of solvent A and solvent B was used. Using a flow of 1.0 mL min^{-1}, solvent B was increased from 0% to 35% in 1 minute, then 35%-40% for 5 minutes, followed by 40%-50% for 3 minutes, and 50%-100% for 2 minutes, this is also shown in Fig. S2a. For the β-pinene SOA extract, the flow rate was set to 0.5 mL min^{-1}, and a mobile phase gradient started at 20% solvent C for 2 minutes, then increased at a rate of 6% min^{-1} up to solvent C of 50%, followed by an increase of 3% min^{-1} to a concentration of 80% solvent C, then 0.75% min^{-1} until 95% solvent C, held at 95% C for 20 minutes and increased by 1.7% min^{-1} to 100%, following 10 minutes at 100% solvent B, shown in Fig. S2b (DeVault et al., 2022).

https://doi.org/10.5194/ar-2023-21
Preprint. Discussion started: 4 January 2024

2.3 Standards for HPLC measurements

Two standard solutions of atmospherically relevant species were made for this study. Standard solution 1 contained 0.4% (by mass) 3-methyl-4-nitrophenol, 0.2% phthalic acid, 0.5% 4-nitrophenol, 0.6% succinic acid, and 0.1% 4-nitrocatechol, dissolved in HPLC grade acetonitrile. Solution 2 contained 8 species: 0.3% phthalic acid (by mass), 0.3% L-malic acid, 0.1% succinic acid, 0.3% citric acid, 0.3% levoglucosan, and 0.2% 4-nitrocatechol in HPLC grade acetonitrile. Source information and calculated saturation mass concentrations for all species are shown in Table S2.

Each species was chosen for its relevance in biomass, urban, or manufacturing processes. 3-methyl-4-nitrophenol, 4-nitrophenol, 4-nitrocatechol and levoglucosan are cyclic C_6 carbon species found in biomass burning. Succinic acid, malic acid, and phthalic acid are non-cyclic acids of secondary origin found in urban atmospheres. Citric acid is found in food and/or medicine. A critical property of these compounds is that they absorb in the UV-Vis, whereas most SOA does not. Nitrates and aromatics have strong absorbance and carboxylic acids have a very weak absorbance.

2.4 Aerosol Generation and Sampling System

The HPLC was coupled to particle phase measurements by using a high-flow Collison atomizer. First, a teflon line was attached to the waste port of the HPLC. The flow from the HPLC was 0.5-1 mL min^{-1}, all of which was sent to the atomizer. The atomizer operated by first introducing pressurized compressed air (~20 psi) into a small chamber (473 ml jar). Perpendicular, sample flow at a rate of 0.5 or 1 mL min^{-1} intersected the pressurized air. This led to the generation of particles of a consistent size distribution, and provided a total flow ranging from 8 to 10 l min^{-1}. Instrument specific flows were measured daily.

Following atomization, ~10 l min^{-1} of aerosol/solvent flow was sent through a Nafion dryer before being sent through an activated carbon denuder. This denuder is in a stainless steel, ~1 inch diameter and 8 inch length tube, composed of activated carbon honeycomb cross-sections. Flow was then sent into each particle instrument. Solvent was efficiently removed (>99.0%, Pagonis et. al. (2021)) using the carbon denuder. Acetonitrile (a solvent used in the HPLC system) was monitored using the EESI. If acetonitrile started to increase, the EESI denuder was regenerated.

Residence times in different parts of the system were estimated to enable synchronizing the aerosol instrument observations with the measured UV-Vis absorbances. Calculations shown in Table S1 suggest that a delay of at least 41 seconds should be observed between the UV-Vis measurement and detection with the aerosol instruments, which is consistent with the measured delay. Retention times for EESI, AMS, and SMPS may differ from each other by 1-2 seconds, depending on the residence times in the tubing. In addition, bypass flows (shown in Fig. 1) were added to the EESI and AMS to reduce residence times in the tubing and thus particle losses or evaporation. These delay differences were handled by shifting instrument data by the delay times.

2.5 Description of particle measurements

https://doi.org/10.5194/ar-2023-21
Preprint. Discussion started: 4 January 2024

2.5.1 Extractive Electrospray Time-of-Flight Mass Spectrometry (EESI)

The EESI uses a soft ionization technique that detects particle-phase analytes based on their solubility and proton affinity/adduct formation stability (Lopez-Hilfiker et al., 2019). Briefly, particle/gas sample flow was sent into the EESI source at ~0.5-1 l min^{-1}, where gases are removed using a charcoal denuder (>99% removal efficiency for acetic acid, when regenerated daily) (Tennison, 1998; Pagonis et al., 2021). The aerosol inlet for the instrument used in this study was pressure controlled (Pagonis et al., 2021), and was run at 766 mbar. While designed for aircraft applications, the pressure-controlled inlet provides better spray and signal stability as it shields the spray from small pressure perturbations from changes in upstream inlet flow conditions such as switching between different sampling modes and plumbing pathways. The working fluid consisted of a mixture of 25% milli-Q water and 75% (by volume) HPLC grade methanol. The EESI was run in two polarity modes. The positive polarity mode (henceforth "EESI+") contained 200 ppm of sodium iodide (NaI) (Pagonis et al., 2021). This working fluid generally forms Analyte-Na^+ adducts. The negative polarity mode (EESI-) was doped with 0.1% (by volume) formic acid (Chen et al., 2006; Gallimore and Kalberer, 2013; Pagonis et al., 2021). Species with a lower proton affinity than formate donate a proton and become negatively charged. This ionization mode is generally sensitive to acidic species that can readily donate a proton and become anionic.

For both polarities, a fused silica capillary (TSP Standard FS tubing, 50 µm ID, 363 µm OD) was used to transport working fluid solution from a pressurized (250-300 mbar above ambient) fluid bottle. Typical resolution at *m/z* 150 was 4000, and mass spectra were saved every second.

The mass concentration of a species (µg m^{-3}) can be quantified from its EESI signal (I_x ion counts s^{-1}) as (Lopez-Hilfiker et al., 2019):

$$Mass_x = I_x\left(\frac{MW_x}{RF_x}\right) \cdot \frac{1}{F} \quad (1)$$

MW_x is the molecular weight of species *x*, *F* is the flow rate (in L min^{-1}), and RF_x is the combined response factor representing fundamental parameters which can be found in Lopez-Hilfiker et. al. (2019). Here, we define a new variable, calibration factor (CF_x^E, in µg m^{-3} $counts^{-1}$ s, such that

$$Mass_x = I_x \cdot CF_x^E \quad (2)$$

Generally, CF_x^E is directly determined by calibrations with standards, when possible. Here, CF_x^E was determined by direct calibrations using either commercially available standards or HPLC-separated analytes. Calibration factors are reported as absolute values (in units of counts s^{-1} μg^{-1} m^3) and also relative to 4-nitrocatechol for EESI- and levoglucosan for EESI+ (unitless).

2.5.2 High Resolution Aerosol Mass Spectrometer (HR-AMS)

A high-resolution time-of-flight aerosol mass spectrometer (hereinafter AMS) (DeCarlo et al., 2006; Canagaratna et al., 2007) was used to obtain 1 Hz chemical composition for organic aerosol (OA) and nitrate aerosol (pNO_3). The

https://doi.org/10.5194/ar-2023-21
Preprint. Discussion started: 4 January 2024

AEROSOL Research Discussions

AMS was run with an inlet flow of 0.1 l min^{-1}, and a bypass flow of ~ 1.3 l min^{-1}. The AMS was run exclusively in "fast mode" (Kimmel et al., 2011; Nault et al., 2018), and size distributions were not recorded. AMS backgrounds were measured for 6 seconds every 52 seconds. Additional backgrounds, in part to test for solvent influence from the HPLC, were taken during the times where no peaks were eluting, and generally remained < 2 µg m^{-3}. The latter were conducted by flowing the sampler air through a particle filter. AMS data was analyzed in the ToF-AMS analysis software (PIKA version = 1.25F, Squirrel = 1.65F) (DeCarlo et al., 2006; Sueper, 2023) within Igor Pro 8 (Wavemetrics, Lake Oswego, OR). The AMS OA relative ionization efficiency (RIE) and collection efficiency (CE) were assumed to be 1.4 ($OA_{default}$, (Canagaratna et al., 2007) and 1, respectively. The AMS NO_3 RIE*CE ($NO_{3,default}$) was assumed to be 1.1 (Canagaratna et al., 2007). Data herein is reported in µg m^{-3}, using Boulder pressure (P=830 mbar) and average lab temperatures (~20°C).

Here, the quantification of different particle-phase species that have been separated by HPLC (and thus are mostly in single component particles) is assessed for the AMS. This is a function of RIE_X*CE_X (a.k.a. "response factor", or CF_x^A) for a species X. Direct AMS calibration has been reported for many OA species (Slowik et al., 2004; Dzepina et al., 2007; Jimenez et al., 2016; Xu et al., 2018; Nault et al., 2023). An RIE of 1.4 is typically applied to ambient aerosols (Canagaratna et al., 2007), which has been shown to perform well in most outdoor intercomparisons (Jimenez et al., 2016; Guo et al., 2021). Laboratory measurements typically require specific calibrations, as RIE can be higher for some compounds and mixtures (Jimenez et al., 2016; Xu et al., 2018; Nault et al., 2023). CE can vary considerably, from CE=0.15 to a CE=1 (Docherty et al., 2013).

The material densities of the known standards were determined by running the AMS in PToF mode and calculating the density as d_{va}/d_m (d_{va} is the aerodynamic vacuum diameter, and d_m is the SMPS measured mobility diameter (DeCarlo et al., 2004)). Calculated densities are shown in table S2. For the unknown species present in the SOA, densities were estimated using the atomic ratio of oxygen plus nitrogen to carbon (O+N:C) and H:C, as demonstrated in Day et. al. (Day et al., 2022), which builds upon the method of Kuwata et. al. (Kuwata et al., 2012) which did not account for nitrate content. The O:C ratio attributed to the non-nitrate OA was calculated per Canagaratna et. al. (2015). The organic nitrate contribution was quantified per Day et. al. (2022). All nitrate here was assumed to be from organic nitrate functional groups, as the aerosol studied here likely contain little inorganic nitrate. For the density calculation, the total nitrate was multiplied by the ratio of the molecular weights of NO_2:NO_3 (46/62) and converted into a molar concentration using the molecular weight of NO_2 (46 g mol^{-1}). Only the NO_2 functionality was included for the density calculation, since the nitrate oxygen bonded to the carbon is expected to typically be included as part of the standard AMS OA O:C estimation (Farmer et al., 2010). Carbon was also converted into a molar concentration using the molecular weight (12 g mol^{-1}). That organic nitrogen to organic carbon ratio was added to the standard AMS OA O:C ratio to obtain the organic nitrate-corrected O+N:C ratio.

For isolated peaks that contained organic nitrate, the organic nitrate (NO_3) concentration was added to the AMS OA to get the total measured AMS mass. The SMPS mass was then compared to the AMS mass calculated with the default CF_x^A, and the correct CF_x^A was determined with Eq. 3 (further details in Sect. 2.7).

$$CF_x^A = \frac{OA\,default + NO_{3,default}}{SMPS\ mass} \quad (3)$$

https://doi.org/10.5194/ar-2023-21
Preprint. Discussion started: 4 January 2024

For HPLC peaks composed of multiple species (like in the β-pinene SOA sample), the average CF_x^A was calculated by adding the average NO_3 contribution (~5%) to the measured AMS OA contribution (Fig. S3). This CF_x^A was then applied to the AMS PMF organic chromatographic time series, in order to determine CF_x^E. For species not containing any nitrate, the $NO_{3,\,default}$ was set to 0.

We note that some recent work has suggested that the sensitivity of organic nitrate functional groups may be lower than for ammonium nitrate (for which the nitrate is calibrated by default in AMS data processing). Thus, a correction of ~62/46 may be more appropriate here for computing nitrate functional group mass concentrations (Takeuchi et al., 2021). However, due to the small nitrate contribution overall, such a correction is not applied.

2.5.3 Scanning Mobility Particle Sizer (SMPS)

Two SMPSs were run with a 20 second offset during HPLC experiments (consisting of all TSI, Inc components) in order to improve the time resolution of the total particle volume measurement. For both SMPSs, a 3081 differential mobility analyzer (DMA) was run with a 3080 Electrostatic Classifier. Each was coupled with either a 3776 condensation particle counter (CPC) (referred to as SMPS A) or a 3775 CPC (SMPS B). Both systems were run in the CPC "high flow" mode. Sample flow rates were nominally set to 1.5 l min^{-1}, but the actual (measured flow) was 1.43 and 1.49 l min^{-1} for the 3776 and 3775, respectively. DMA sheath flows were set to 6.0 l min^{-1}. Data were compared to that acquired in a reference mode, with a sample flow of 0.3 l min^{-1}, a sheath flow of 3.0 l min^{-1}, and 120 s scans. Testing was done to ensure that number and volume distributions and integrated concentrations matched between the reference and fast scanning modes, shown in Fig. S4 and discussed in depth in Sect. S3. The SMPSs were also run concurrently during an HPLC run to confirm that data from both instruments matched (Fig. S5). Overall, the SMPSs in the reference and fast modes agreed within 10%. Flows were measured every day, and delay times (from the SMPS inlet to the CPC detection, which affect sizing) were calculated when changes in plumbing were made. Further details on SMPS delays can be found in Table S3.

2.6 Positive Matrix Factorization (PMF)

Positive Matrix Factorization (PMF) (Paatero and Tapper, 1994; Paatero, 1997) is a bilinear deconvolution model that relies on the assumption of mass balance with components with constant spectral profiles. Briefly, time series for signals at individual *m/z*'s are entered into a two-dimensional matrix with *m* rows (points in time) and *n* columns (*m/z*'s) (Ulbrich et al., 2009; Kumar et al., 2022). PMF works to minimize the squared weighted residuals between the measured and reconstructed matrices, producing multiple potential solutions that could explain different chemical or physical sources in a given data set, along with the total residual of each solution.

The model is solved using PMF2 (Paatero, 2007) and the multilinear engine, developed by Paatero et. al. (1999), run from the PMF Evaluation tool ("PET") software v3.08 in Igor Pro v8 (Wavemetrics, Lake Oswego, OR). Choosing the best PMF solution always has a subjective component, as it is usually impossible to know the "correct" number of factors that completely capture a complex data-set (Ulbrich et al., 2009). Several methods can be used to assess the validity of a given solution. First, the Q-value (Q), which is the total sum of the error-weighed square residuals for a data set, is used. Q_{exp} is the expected value of Q if all residuals are due to random errors with

https://doi.org/10.5194/ar-2023-21
Preprint. Discussion started: 4 January 2024

the estimated precision at each point. If the individual data points in a solution are fit so that the residuals are consistent with random noise, then $Q/Q_{exp} \sim 1$. Note that this also requires accurate estimation of the precision (random error) in the entire data matrix. In some situations, PMF cannot explain a data set within an acceptable error. In these situations, $Q/Q_{exp} >> 1$. All solutions here have $Q/Q_{exp} \leq 1$.

The second criteria for picking the best PMF solution is by exploring the time series and mass spectra for a given solution for different approximate rotations (FPEAK values) (Lee et al., 1999; Lanz et al., 2007; Ulbrich et al., 2009). Simply, PMF rotations are non-unique solutions that are represented across multiple factors. In a real-world example, a source profile (for example, biomass burning OA), might split across multiple PMF factor's time series and/or mass spectra, despite only being from a singular source. Factor splitting can sometimes reduce residuals, and mathematically may appear as a more correct solution for a particular dataset. This is where the user must thoroughly assess different solutions, specifically those with $Q/Q_{exp} \sim < 1$.

PMF solutions chosen here are based on the above criteria and a third: the time series of the residuals. In a chromatogram, the shape of the peaks are generally known. Here, 4 different instruments generate unique chromatograms: UV-Vis, HRAMS, EESI, and the SMPSs. Thus, across those four instruments, the shape of the chromatogram was fairly well constrained. When choosing solutions here, the shape of the chromatogram was compared to the time series of the residuals. If the residuals showed significant peaks, then that was an indicator that not enough factors were used to represent the complete chromatogram and all of the factors therein.

The *m x n* matrix for AMS data was generated for HR ions using the PMF export option in the PIKA data analysis software. Briefly, unit mass and high resolution AMS data were first fit as described in Sect. 2.5.2. After confirming that all ions of interest were well fit, the organic data was exported into an *m x n* matrix (both signal and precision matrices). Any HR ions not associated with the following families: C_x, CH, CHO_1, and CHO_{gt1} were removed, as NO_3 was not included in the PMF input, and the included families were the only measured ions with substantial signal during the experiments included here. PMF was run from 1-20 factors. Rotations (FPEAKS) were enabled, ranging from -1.0 to 1.0, in steps of 0.2.

2.7 Calculating calibration factors for species using the multi-instrumental method

For unknown species (or known species with an unknown AMS response factor) the following method was used to obtain EESI and AMS calibration factors:

1. Calculation of composition-dependent density using the measured elemental composition or d_{va}/d_m measured densities.
2. SMPS size distributions are fit with a lognormal curve, and integrated volume concentrations are obtained.
3. SMPS integrated volume time series were multiplied by the density, to produce the reference mass concentration time series.
4. The high-time-resolution AMS OA and NO_3 time series are obtained for an assumed RIE*CE=1.4 ($OA_{default}$) and RIE*CE=1.1 ($NO_{3,\ default}$).
5. The SMPS mass concentration time series and the AMS OA+NO_3 time series, for an individual chromatographic peak, are fit with a Gaussian distribution

https://doi.org/10.5194/ar-2023-21
Preprint. Discussion started: 4 January 2024

6. The AMS and SMPS Gaussian distributions are integrated (µg m^{-3} s).
7. The CF_x^A was obtained using the ratio of the integrated SMPS to the integrated AMS time series fits (Eq. 3).
8. The time series for the EESI *m/z* was fit with a Gaussian and integrated along the retention time.
9. The integrated gaussian for the EESI *m/z* was divided by the integrated AMS ($OA+NO_3$, after AMS calibration by the SMPS) or SMPS gaussians to obtain CF_x^E (counts s^{-1} m^3 μg^{-1}).

https://doi.org/10.5194/ar-2023-21
Preprint. Discussion started: 4 January 2024

3 Results

3.1 Mass Balance of the Analyte in the Experimental System

There was substantial plumbing between the injected sample and the instruments measuring the analyte, where losses can occur (Fig. 1, Table S1). In order to better understand the experimental system, the mass flux was calculated using the known, injected mass as well as the tubing diameters, lengths, and flow rates, as shown in Fig. 2.

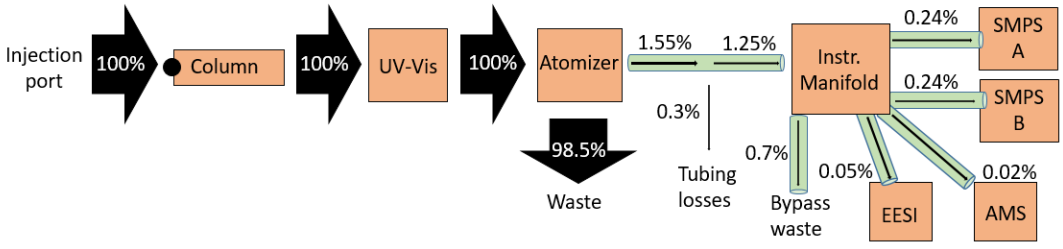

Figure 2. Mass flux across the multi-instrumental setup. Arrows are sized by the percentage of analyte mass, which is included alongside each arrow. EESI and AMS have bypass lines (represented as the total by 0.7% bypass waste). Percentages shown are for the actual measured mass percent. Tubing details are also included in Fig. 1.

By injecting a known amount of sample into the HPLC column, we were able to account for all the measured mass by the four instruments sampling. As shown in Fig. 2, all of the injected mass was analyzed by the UV-Vis spectrometer, but only a small fraction of it was analyzed (0.55%) by the online instruments. There was substantial fluid loss at the atomizer, which is thought to account for the bulk of the mass leaving the HPLC. The EESI and AMS measure the least mass, due to their low flow rates (0.28 l min^{-1} and 0.1 l min^{-1}, respectively). Of the mass that exited the atomizer, ~20% was lost in the tubing (~10 m, ¼" I.D.) to the aerosol sampling manifold (represented as 0.3% of total in Fig. 2). Overall, the efficiency in sampling the injected mass with the online instruments was very low with this system, primarily due to the atomization process. In SOA extracts that are highly concentrated, this is not a major problem. However, application of this method to lower concentration samples would benefit from use of a lower-flow liquid chromatography method and a more efficient atomizer.

3.2 Application of multi-instrumental method and PMF for standard species' calibrations

3.2.1 Cross comparison between directly calibrated one-component chromatographic standards vs. multi-instrumental method

In order to test the efficacy of the proposed method, two solutions were made containing one standard each (phthalic acid and 4-nitrocatechol). These species were first calibrated directly in order to obtain CF_x^E and CF_x^A. Direct

https://doi.org/10.5194/ar-2023-21
Preprint. Discussion started: 4 January 2024

calibration hereout refers to the standard method of generating monodisperse aerosol from a calibrant solution with a Collison atomizer (TSI model 3076) drying with a Nafion dryer, size selecting at 275 nm with a 3080 electrostatic classifier / 3081 DMA, removing double-charged particles with an impactor, measuring the particle concentration with a 3775 CPC, and measuring with the EESI and/or AMS. Then, each solution was injected into the HPLC to generate isolated chromatograms (Fig. 3).

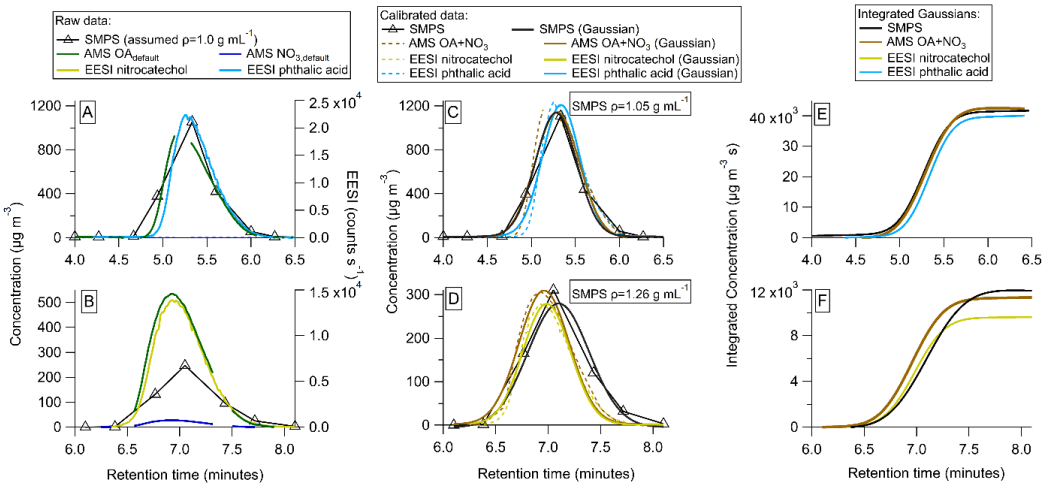

Figure 3. (A) Uncalibrated data collected during a single standard (phthalic acid) HPLC run, (B) raw data from a nitrocatechol HPLC run, (C) calibrated phthalic acid data (using the monodisperse calibration factors), (D) calibrated nitrocatechol data, (E) integrated Gaussian peaks from (C), and (F) integrated Gaussian peaks from (D).

In Fig. 3a, the uncalibrated background-subtracted data is shown. Phthalic acid contains no nitrate moiety, so AMS NO_3 was 0. Fig. 3b shows the raw data for 4-nitrocatechol. Due to the nitro group, AMS NO_3 is added to AMS OA to obtain the total mass measured by the AMS. If the method was followed as described in Sect. 2.7, the raw data would be fit with Gaussian curves and integrated, in order to produce CF_x^E and CF_x^A for each species. However, in this test study, CF_x^E and CF_x^A are already known.

Figure 3c shows the directly calibrated (as opposed to the multi-instrumental approach calibrated) data for phthalic acid. It is clear that the AMS, EESI, and SMPS data line up well, indicating that the multi-instrumental approach produces very similar CF_x^E and CF_x^A as the direct calibrations. Fig. 3d echoes this, showing good overlap across each instrument for nitrocatechol.

Figures 3e and 3f show the integrated, calibrated Gaussian curves. If the multi-instrumental method worked as well as direct calibrations, the maximum integrated values would be expected to be the same for each instrument. For phthalic acid, the instruments agree within 6%, with the EESI showing the largest deviation from the other instruments. For 4-nitrocatechol, this difference is 20%, and again the EESI is the farthest from the other instruments. Such discrepancies could be due to changes in EESI sensitivity, which may be driven by the different solvents used for calibration (water for direct calibrations, and a mixture of acetonitrile and water for the multi-

https://doi.org/10.5194/ar-2023-21
Preprint. Discussion started: 4 January 2024

instrumental method). It could also be due to the high concentrations of each solute, which may change CF_x^E slightly.

Following method validation through comparison between direct calibrations and the multi-instrumental calibration method, a mixture containing five standards (phthalic acid, 4-nitrocatechol, succinic acid, 4-nitrophenol, and 3-methyl-4-nitrophenol) was run through the HPLC column (Fig. 4). Like above, each species was first calibrated directly, in order to compare the direct calibration values vs. the multi-instrumental calibration method for a more complex chemical system.

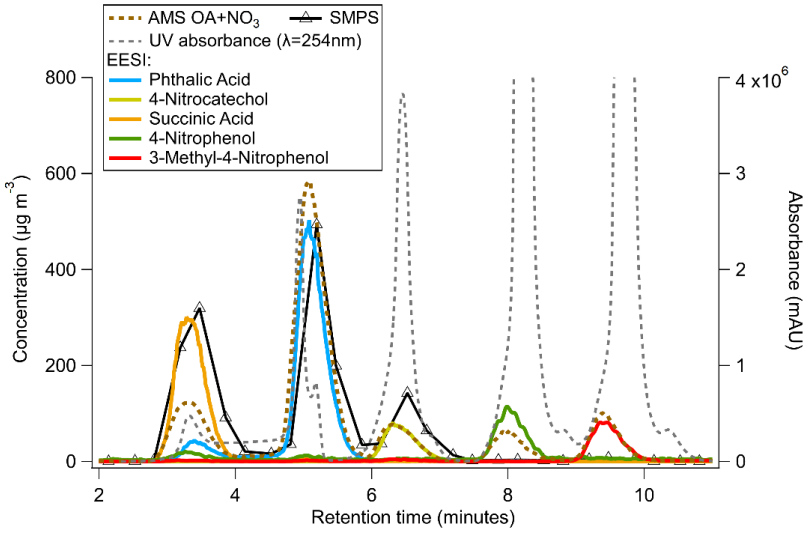

Figure 4. Time series of UV absorbance (milli-absorbance units) and AMS, EESI, and SMPS mass concentrations for a mixed-solution standard HPLC run.

In Fig. 4, succinic acid was the first peak to elute from the HPLC column, from ~2.5-4 minutes. The EESI and SMPS data match well, but the AMS data is lower by a factor of ~2. This is potentially driven by the phthalic acid/succinic acid co-elution (as evidenced by the EESI). The CF_x^A for both species is shown in Table 1. CF_x^A differ substantially, and an internal mixture of aerosols containing succinic acid and phthalic acid may result in a larger AMS bias (as $CF^A_{Succinic\ Acid}$ and $CF^A_{Phthalic\ Acid}$ differ significantly) than the EESI (where we measured molecular ions) or the SMPS (as the density of phthalic acid and succinic acid are similar, table S2).

https://doi.org/10.5194/ar-2023-21
Preprint. Discussion started: 4 January 2024

AEROSOL Research Discussions

Table 1. Calibration factors for resolved (or mostly resolved) standard species. CF_x^E values are reported in counts s^{-1} μg^{-1} m^3 and the relative EESI calibrations factors (CF_x^E/CF_{nitro}^E (EESI-) or CF_x^E/CF_{levo}^E (EESI+)), and the AMS calibration factors (CF_x^A)are unitless values.

Species	Direct calibration CF_x^E (counts s^{-1} μg^{-1} m^3)	Multi- instr. calibration CF_x^E (counts s^{-1} μg^{-1} m^3)	Direct calibration CF_x^E/CF_{nitro}^E (EESI-) or CF_x^E/CF_{levo}^E (EESI+)	Multi- instr. calibration CF_x^E/CF_{nitro}^E (EESI-) or CF_x^E/CF_{levo}^E (EESI+)	Direct calibration CF_x^A (unitless)	Multi-instr. CF_x^A (unitless)
4-nitrocatechol (EESI-)	44.1±5	23	1	1	1.96±0.17	1.05
4-nitrocatechol (EESI+)	-	18	-	0.020	-	-
Succinic Acid (EESI-)	30±4.0	22	0.68	0.98	1.6±0.10	0.52
Succinic Acid (EESI+)	-	26	-	0.029	-	-
Phthalic Acid (EESI-)	18.1±2.8	18	0.41	0.82	0.79±0.070	1.0
Phthalic Acid (EESI+)	-	620	-	0.68	-	-
4-nitrophenol (EESI-)*	1.6±0.57	26	0.036	1.2	0.59±0.050	5.9
3-methyl-4-nitrophenol (EESI-)*	5.8±4.0	42	0.14	1.9	0.90±0.10	8.0
Levoglucosan (EESI+)	200±10	900	1	1	0.45±0.06	-

* The reported values here are highly uncertain due to differences in evaporation for each instrument

Phthalic acid elutes as two isomers, with the largest eluting between 4 and 6 minutes. All three instruments match well. 4-nitrocatechol was next, and showed very good agreement between the EESI and AMS, but a factor of ~2 difference between the SMPS and AMS/EESI. The exact cause for this discrepancy is unknown.

4-nitrophenol and 3-methyl-4-nitrophenol both match well between the EESI/AMS, but the SMPS concentration is a factor of 20 less than the other two instruments. The likely explanation is that 4-nitrophenol and 3-methyl-4-nitrophenol are volatile (table S2). Compared to succinic acid, >90% of these species evaporated from injection to detection by the EESI/AMS. The SMPS measurement is slower than the other instruments, and dilutes the incoming aerosol by a factor of 4 inside the DMA column. The AMS and EESI measurements are faster and do not dilute the incoming aerosol. Due to these differences, nearly all of the injected mass evaporated in the SMPS.

https://doi.org/10.5194/ar-2023-21
Preprint. Discussion started: 4 January 2024

This suggests that volatile species (where C* >> OA) are not able to be calibrated for by this method. Evaporation would also likely occur during direct calibrations, but to a lesser degree due to the higher pure-species OA concentrations.

3.2.2 Combined application of the multi-instrumental calibration method and PMF on two mixed standards solutions

PMF was combined with the multi-instrument calibration method to better separate succinic acid and phthalic acid, which overlap in Fig. 4. The results of applying PMF to the AMS data is shown below in Fig. 5. A 6-factor solution was chosen (Fig. 5g).

https://doi.org/10.5194/ar-2023-21
Preprint. Discussion started: 4 January 2024

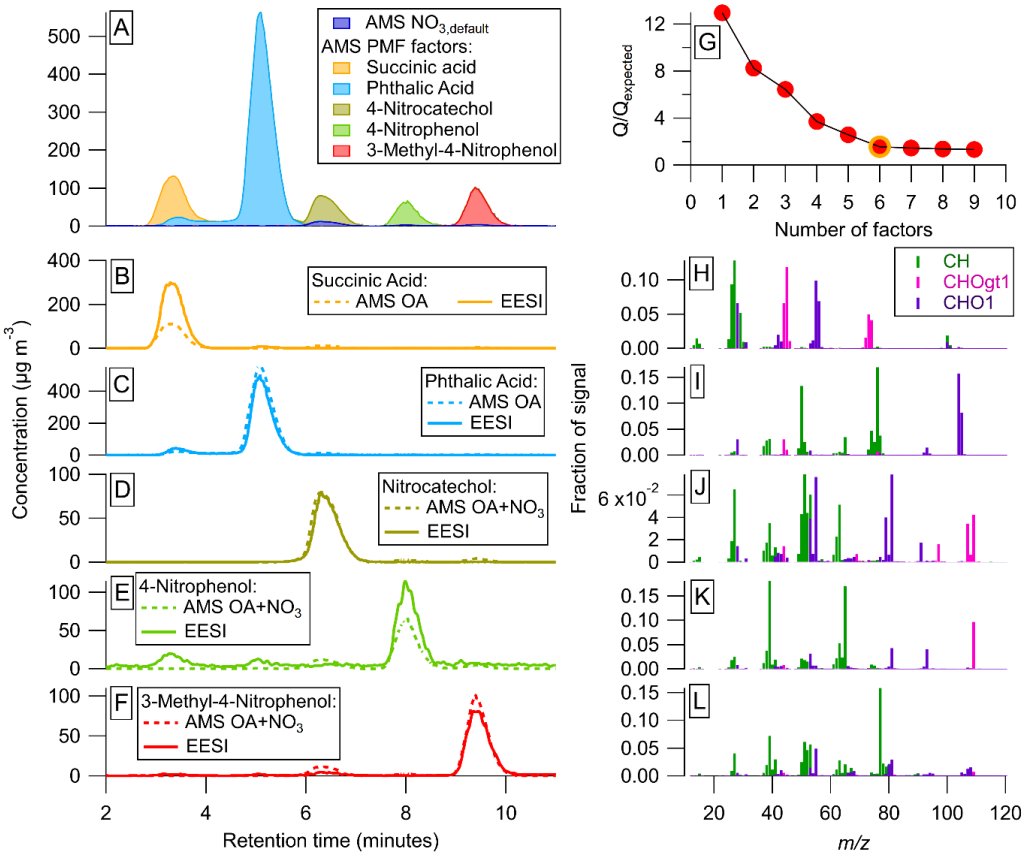

Figure 5. Time series for the PMF solution, (A) stacked plot of each factor and AMS NO_3, (B)-(F) PMF factor with CF_x^A applied to individual species, along with EESI concentrations. (G) $Q/Q_{expected}$ vs. number of PMF factors, chosen solution circled in yellow. (H)-(L) mass spectra (colored by associated AMS HR family) for each AMS PMF factor.

Figure 5a-5f show excellent separation by PMF between the time series for each of the standards present in the mixture. This is likely due to the very different mass spectra for each species (Fig. 5h-5l) as well as the time separation achieved by the HPLC. The mass spectra for each standard was compared to the direct calibration mass spectra to confirm the PMF factors were assigned correctly (Fig. S6 and table S4). For all species, there was excellent correspondence, and the uncentered correlation coefficient (UC) between the mass spectral peaks was >0.95.

Here, the CF_x^A and CF_x^E values are known for each pure standard (from direct calibrations). When applying the *CF* to individual species, the overall agreement between the AMS and EESI time series is comparable to that shown in Fig. 4. The AMS still underestimates succinic acid by a factor of ~2 compared to the EESI, even after better separation is achieved with PMF. As discussed previously, this could be due to the mixing of the two species, which might change the viscosity or phase of the sampled aerosols compared to the pure species, which in turn

https://doi.org/10.5194/ar-2023-21
Preprint. Discussion started: 4 January 2024

could fundamentally change the CF_x^A due to the change in CE. Whilst separation was achieved with PMF, PMF time series are likely more accurate for systems where different species have similar CF_x^A (e.g. SOA mixtures from a single precursor and oxidant).

The mixture studied in Fig. 4 and Fig. 5 was mostly well-separated without PMF. In order to assess the ability of PMF to separate a more complex mixture, PMF was run on a different standard solution shown in Fig. 6.

https://doi.org/10.5194/ar-2023-21
Preprint. Discussion started: 4 January 2024

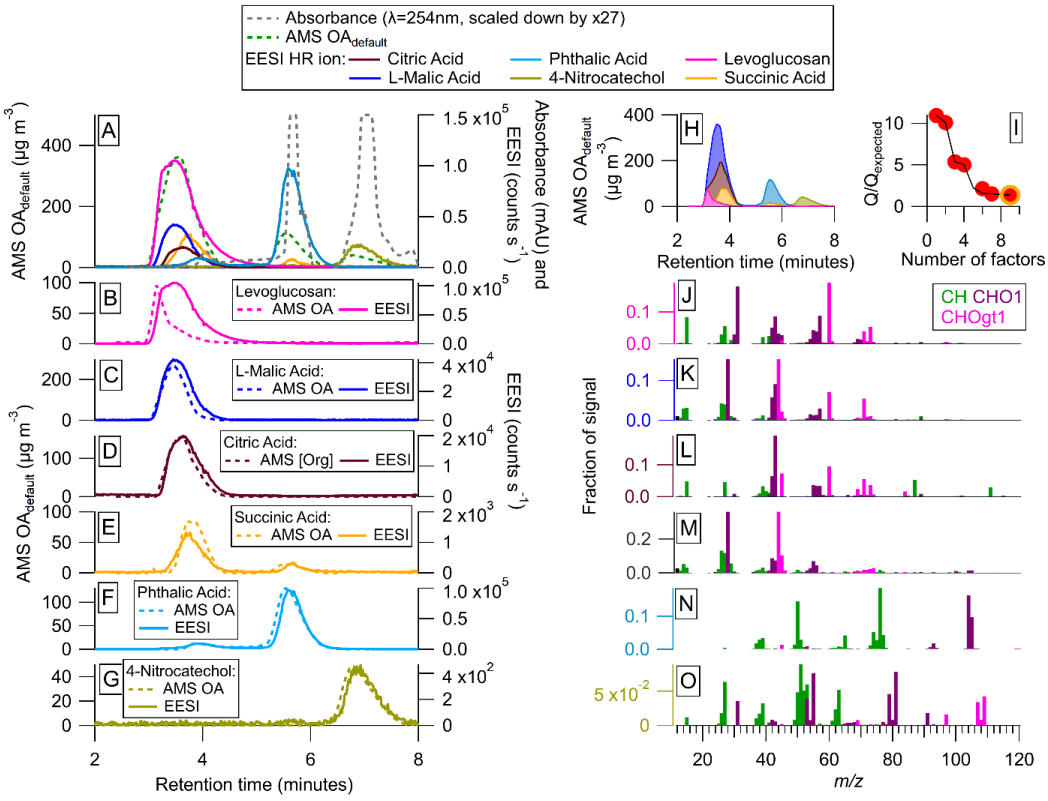

Figure 6. (A) time series of AMS total OA (assumed CF_x^A=1.4), EESI HR ion, and absorbance (max=4✕10^6, milli-absorbance units). (B)-(G) AMS PMF factor (assumed $CF_x^{A,default}$=1.4) and EESI HR ion for 6 calibrants. (H) Stacked PMF factor solution time-series, (G) Q/Q$_{expected}$ for AMS PMF solution, a 9-factor solution was chosen (yellow circle) with FPEAK=0.2, and (J)-(O) AMS family-colored mass spectra for 6 PMF factors.

Unlike the data shown in Fig. 3-5, the species run in the standard solution shown in Fig. 6 were not calibrated directly. Thus, Fig. 6 serves as a test of PMFs ability to resolve complex mixtures, rather than a comparison of the calibration methods. Figure 6a shows the uncalibrated time series/chromatogram for the standards in the mixture. In contrast to the previous mixture, this solution contains 5 co-eluting peaks: levoglucosan, L-malic acid, citric acid, succinic acid, and a small fraction of the phthalic acid and its isomer. These 5 co-eluting peaks suggest that the application of only HPLC with the separation method being used here is not sufficient for these species, likely due to how polar they are. Further separation could be achieved by either changing the HPLC method (through the use of a normal phase chromatography, which uses e.g. a silica column) or running PMF on the AMS data.

Figures 6b-6h shows PMF time series for the standards present in the mixture. In Fig. 6b, both the AMS and EESI levoglucosan peaks have different shapes. The EESI peak has a right tail, which is potentially due to the "sticky" (semi-volatile) nature of levoglucosan (Brown et al., 2021). The AMS peak has a sharp increase and slow

https://doi.org/10.5194/ar-2023-21
Preprint. Discussion started: 4 January 2024

descent, and does not resemble a Gaussian (which is the approximate shape we expect eluting peaks to have). This is likely due to an imperfect PMF separation. Despite that, when comparing the mass spectra in Fig. 6j to the direct calibration mass spectra in Fig. S7, UC (table S5) is 0.93, suggesting consistency between the two mass spectra.

L-malic acid and citric acid also co-elute with levoglucosan. The PMF factors assigned to those species do look like Gaussian curves, but the mass spectra shown in Fig. 6j-6l are somewhat similar. The assigned malic acid factor has a UC of 0.89 with the directly calibrated mass spectra, but citric acid was not directly calibrated for, and it is likely there is some overlap in the AMS factors between those three species. This was an especially complex solution for PMF to resolve due to the very similar retention times and mass spectra between these species.

As in Fig. 5, succinic acid, phthalic acid, and 4-nitrocatechol (Fig. 6e-6g and Fig. 6m-6o) are easily resolved when running PMF on the HPLC chromatograms. This is likely due to both the retention time differences and the different AMS mass spectra for these three species. In Table 1, calibration factors are shown for levoglucosan, succinic acid, phthalic acid, and 4-nitrocatechol. CF_x^A is known from the direct calibrations done in Fig. 4. Only levoglucosan was cross-calibrated with a direct calibration, but the multi-instrumental calibration value is highly affected by the shape of the AMS PMF factor associated with levoglucosan. Thus, the multi-instrumental calibration factor for levoglucosan is likely incorrect. The PMF factor stacked time series is shown in Fig. 6h.

3.3 Combined application of the multi-instrumental calibration method and PMF on β-pinene/NO_3 SOA

In order to test the applicability of the proposed method to a complex real system, SOA from β-pinene + NO_3 was generated, collected on a filter, extracted, and analyzed with our multi-instrument system (per Sect. 2.1). This SOA system has been studied in depth previously and many of the products have been identified (Claflin and Ziemann, 2018; DeVault et al., 2022). The HPLC method was that of DeVault et al. (2022). Species here are identified based on comparison to the results in the aforementioned papers, and the observed EESI+ HR ions that show peaks in the time series (Fig. 7). Per Claflin and Ziemann (2018), many of the known products are oligomers, formed primarily from the reactions of two carbonyl nitrate monomers. For simplicity, the SOA peaks observed will be referenced by their associated EESI HR ion.

https://doi.org/10.5194/ar-2023-21
Preprint. Discussion started: 4 January 2024

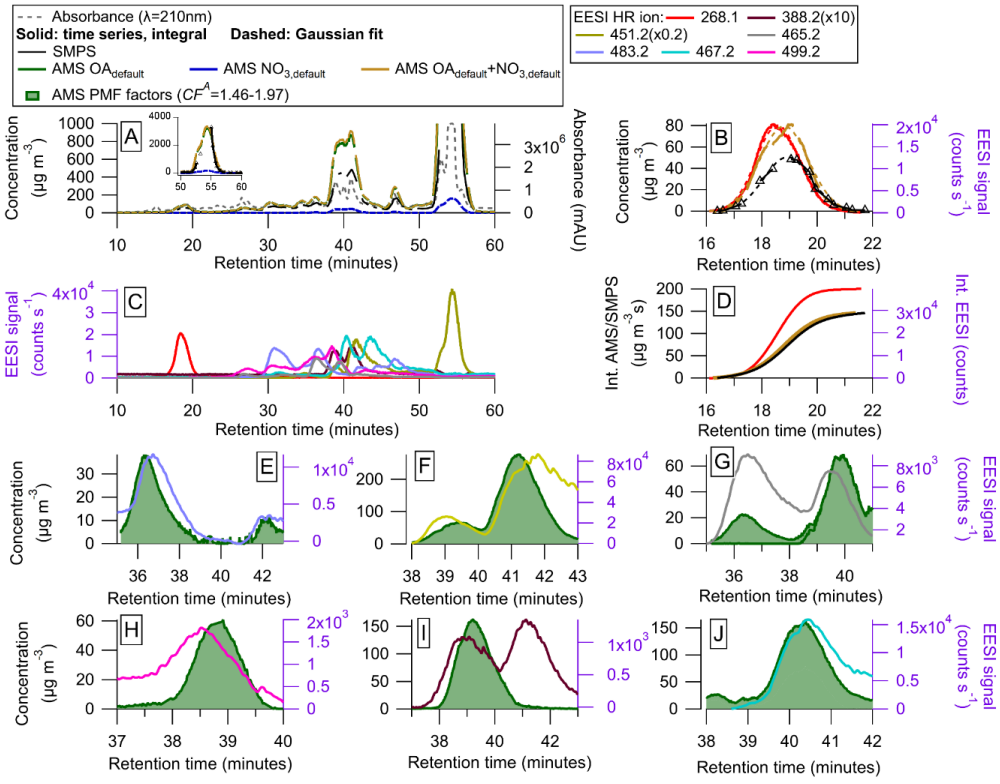

Figure 7. Results of an HPLC run for SOA from β-pinene + NO_3 (A) AMS, SMPS, and UV-Vis chromatograms (milli-absorbance units), with inset showing peak from 50-60 minutes. (B) Time series and Gaussian fits for the peak between 16 and 20 minutes (without using PMF), (C) EESI HR ions time series (D) time integrated mass concentrations (ion signal) for AMS OA and NO_3, SMPS total mass, and EESI+ HR ion (m/z=268.1). (E)-(J) show AMS PMF factors against measured EESI+ HR ions. (G), (I), and (J) represent split AMS PMF factors for the measured EESI+ HR ions. The AMS PMF factors have a CF_x^A ranging from 1.46-1.97 as shown in Fig. S3 and Table 2. Densities are applied to the SMPS data, shown in Fig. S8.

Figure 7a shows the full time-series for the β-pinene system. Many chromatographic peaks are observed by the AMS, SMPS, EESI, and UV-Vis. Many of the peaks are present in clusters and not well enough resolved to fit individual Gaussian curves to the EESI and AMS data. Claflin and Ziemann (2018) measured a similar (albeit slightly better separated) UV-Vis chromatogram (Fig. S9). Differences could potentially arise due to the age of the SOA extract used here (~ 1 year) vs. the fresh SOA extract used in that study, or other experimental factors.

Overlapping peaks are also observed in the EESI data (Fig. 7c). There are two isolated peaks, from 15-21 minutes and 52-58 minutes. One peak, measured at EESI HR ion m/z 483.2 (suspected structure shown in table S6), was mostly resolved, and also shows up from ~46-48 minutes. The raw (and fitted) data is shown in Fig. 7b for the

https://doi.org/10.5194/ar-2023-21
Preprint. Discussion started: 4 January 2024

EESI ion measured at *m/z* 268.1 (a monomer, tricarbonyl nitrate) (Claflin and Ziemann, 2018). The integrated fits are shown in Fig. 7d.

Multiple peaks overlap from ~30 to ~50 minutes (based on the EESI data shown in Fig. 7c). These peaks are likely all dimers, the species identified by Claflin and Ziemann (2018) and measured by the EESI are shown in Table 5. Not every peak observed in Claflin and Ziemann (2018) was identified here, which is likely due to lack of EESI sensitivity to some species and potential decomposition of SOA products (specifically for the trimer identified in Claflin and Ziemann (2018)). In contrast, some EESI HR ions that do not correspond to peaks identified in Claflin and Ziemann (2018) were detected here, but structures for those species are unknown.

In Fig. 7e-7j, AMS PMF time series for the middle third of the run are shown alongside EESI HR ions. The full PMF solution can be found in Fig. S10-S12. AMS factors were matched with EESI HR ions based on the retention time and general shape of the time series. For some peaks, the retention times differ by up to 0.5 min. These peaks are assigned based on the similarity in time series between the EESI and AMS. The complexity of this solution, as well as the similarities in the products' molecular structures, likely hindered the ability of PMF to fully resolve each individual product. For the peaks that overlap the most in time, the magnitude of the individual AMS PMF factors separated during this time are comparable to each other.

CF_x^E and CF_x^A are given for each identified species in Table 2. Many of the identified species have CF_x^E in the same range as levoglucosan, within a factor of 3.

Table 2. EESI HR ion, CF_x^E (counts s^{-1} μg^{-1} m^3), CF_x^E/CF_{levo}^E, CF_x^A, and associated PMF factor for the β-pinene + NO_3 SOA mixture. CF_{levo}^E= 441.6 counts s^{-1} μg^{-1} m^3. CF_x^E was calculated using the AMS PMF [Org]×1.05 (the average [NO_3] contribution was ~5%, Fig. S3).

EESI ion	CF_x^E (counts s^{-1} μg^{-1} m^3)	CF_x^E/CF_{levo}^E (unitless)	CF_x^A (unitless)	**AMS PMF factor(s)**
268.1	270	0.61	1.46	-
388.2	10.9	0.023	1.97	9, 13
451.2 (1)	407	0.92	1.97	13
451.2 (2)	423	0.96	1.73	13
451.2 (3)	83.2	0.19	1.97*	-
465.2 (1)	670	1.5	1.97	2
465.2 (2)	170	0.38	1.97	10
467.2	139	0.31	1.73	5,8
483.2	435	0.99	1.97	14
499.2	54.2	0.12	1.97	12

* Incomplete SMPS data, assuming CF_x^A=1.97.

https://doi.org/10.5194/ar-2023-21
Preprint. Discussion started: 4 January 2024

Some species, like the EESI HR ions measured at *m/z* 388.2 and *m/z* 499.2 have much lower EESI sensitivity than the other species. These species could be fragments of a larger parent ion, or they could be species that, for whatever reason, do not form a strong adduct with Na^+. The ambiguity in the PMF factors may result in some errors in CF_x^E, but they are unlikely to fully explain the factor of ten difference in sensitivity between the most and least sensitive β-pinene+NO_3 products. In future runs with slightly better chromatographic separation a multi-variate fit of individual factors vs. the SMPS may allow further constraining the quantification.

In this system, many of the products differ only by one or two oxygens. Some may contain a carboxylic acid functional group in the place of a ketone, whilst others contain a cyclic ether, and some do not. The subtle differences in structure could influence the sensitivity with the EESI, as the oxygenated moieties may change the likelihood of forming a strong $[M+Na]^+$ adduct. Further, some EESI HR ions elute multiple times (e.g. *m/z* 451.2). Claflin and Ziemann (2018) identified the structure of this ion for the third peak (Table S6). However, this ion is measured twice more, from 38-43 minutes. Due to the chromatographic separation between these peaks and the third peak, it is likely that the first two species are some isomeric form of the species identified in Claflin and Ziemann (2018). As is shown for *m/z* 483.2 (Table S6), isomers can have different structures and very different CF_x^E (327.2 vs. 54.2 counts s^{-1} μg^{-1} m^3).

Despite differences in CF_x^E, CF_x^A was more consistent. For the mixed peaks (individual EESI *m/z*'s shown in Fig. 7e-7j), CF_x^A was either 1.48 or 1.58, as shown in Fig. S3. For the three isolated peaks (*m/z* 268.2, *m/z* 451.2 [peak 3], and *m/z* 483.2 [peak 2]), the CF_x^A spanned from 1.31 to 1.75. For one of the isolated peaks, *m/z* 451.2 (peak 3), the actual CF_x^A was not calculated, due to a malfunction of the SMPS system between 54-56 minutes. Individual peaks' Gaussian fits and integrated curves are shown in Fig. S13.

4 Conclusions

A multi-instrumental calibration method has been demonstrated here, that uses the chemical separation power of the HPLC, combined with analytical aerosol detection of SMPS, AMS, and EESI to calibrate the mass spectrometers for individual species in mixtures. When running individual standards, the multi-instrumental calibration method agreed with direct calibration within 20%. As the sensitivities of EESI measured species can vary by over an order of magnitude, quantification within 20% is very useful. In a mixed standard run that contained mostly resolved species, the EESI and SMPS agreed within a factor of 1.5 (for non-volatile species). The AMS and EESI matched moderately well, except when measuring succinic acid.

In situations where the HPLC column/method was unable to fully separate injected components, PMF was used to methodically compare the time series and mass spectra for different species, and generate time resolved OA data for the AMS. This was especially important for the AMS data, as overlapping peaks are measured as large and wide "total OA" peaks for that instrument.

The β-pinene SOA solution was the most complex mixture studied here, primarily due to the suspected presence of many isomers. The majority of the SOA peaks overlapped during the middle third of the HPLC run. PMF separation conducted on the HPLC-separate AMS results produced a more complicated solution than the AMS

https://doi.org/10.5194/ar-2023-21
Preprint. Discussion started: 4 January 2024

PMF done on the standards' runs. This was likely due to similarities in mass spectra and retention times for the overlapping peaks. Despite that analytical challenge, when the middle third of the chromatogram was scrutinized using both the AMS PMF solution and the measured EESI+ HR ions, approximate calibration factors were obtained.

For future studies, additional effort should be focused on tuning the HPLC performance (e.g. through changing the column or mobile phase gradients) that provides higher resolution for whatever system is being studied. In this demonstration project we were limited to a C_{18} column, which is most often used for less polar species. In many situations, especially when there is significant oxidation and smaller precursor gases, the resulting products are likely to be more polar than can be separated by a C_{18} column. In future experiments, columns with more polar stationary phases should be considered. If HPLC separation alone could completely resolve all chemical peaks, then PMF would not be needed, however in practice it is likely to help the chemical resolution of complex systems.

These results introduce a new technique for better quantifying the instrument responses of the EESI and AMS to different molecular species present in complex mixtures such as from biomass burning, urban, and/or biogenic SOA.

5 Acknowledgements

We thank Harald Stark for data analysis support for Igor and Tofware. This work was supported by NASA grants 80NSSC18K0630, 80NSSC23K0828, and 80NSSC21K1451, a NASA Future Investigators in Earth and Space Science and Technology graduate student research grant (FINESST, 80NSSC20K1642), NSF AGS-2206655, and a CIRES graduate research fellowship.

6 Author Contributions

MKS, DAD, JLJ, and PJZ designed the experiments, MKS carried them out with support from DAD, DK, SY, and PCJ. ACZ, PJZ, and MPD provided the HPLC instrument support. MKS carried out all data analysis and preparation of the manuscript, with contributions from all coauthors.

7 Competing Interests

The authors declare that they have no conflict of interest.

https://doi.org/10.5194/ar-2023-21
Preprint. Discussion started: 4 January 2024

References

Bakker-Arkema, J. G. and Ziemann, P. J.: Minimizing Errors in Measured Yields of Particle-Phase Products Formed in Environmental Chamber Reactions: Revisiting the Yields of β-Hydroxynitrates Formed from 1-Alkene + OH/NOx Reactions, ACS Earth Space Chem., 5(3), 690–702, doi:10.1021/acsearthspacechem.1c00008, 2021.

Brown, W. L., Day, D. A., Stark, H., Pagonis, D., Krechmer, J. E., Liu, X., Price, D. J., Katz, E. F., DeCarlo, P. F., Masoud, C. G., Wang, D. S., Hildebrandt Ruiz, L., Arata, C., Lunderberg, D. M., Goldstein, A. H., Farmer, D. K., Vance, M. E. and Jimenez, J. L.: Real-time organic aerosol chemical speciation in the indoor environment using extractive electrospray ionization mass spectrometry, Indoor Air, 31(1), 141–155, doi:10.1111/ina.12721, 2021.

Canagaratna, M. R., Jayne, J. T., Jimenez, J. L., Allan, J. D., Alfarra, M. R., Zhang, Q., Onasch, T. B., Drewnick, F., Coe, H., Middlebrook, A., Delia, A., Williams, L. R., Trimborn, A. M., Northway, M. J., DeCarlo, P. F., Kolb, C. E., Davidovits, P. and Worsnop, D. R.: Chemical and microphysical characterization of ambient aerosols with the aerodyne aerosol mass spectrometer, Mass Spectrom. Rev., 26(2), 185–222, doi:10.1002/mas.20115, 2007.

Canagaratna, M. R., Jimenez, J. L., Kroll, J. H., Chen, Q., Kessler, S. H., Massoli, P., Hildebrandt Ruiz, L., Fortner, E., Williams, L. R., Wilson, K. R., Surratt, J. D., Donahue, N. M., Jayne, J. T. and Worsnop, D. R.: Elemental ratio measurements of organic compounds using aerosol mass spectrometry: characterization, improved calibration, and implications, Atmos. Chem. Phys., 15(1), 253–272, doi:10.5194/acp-15-253-2015, 2015.

Chen, H., Venter, A. and Graham Cooks, R.: Extractive electrospray ionization for direct analysis of undiluted urine, milk and other complex mixtures without sample preparation, Chem. Commun. , (19), 2042–2044, doi:10.1039/B602614A, 2006.

Claflin, M. S. and Ziemann, P. J.: Identification and Quantitation of Aerosol Products of the Reaction of β-Pinene with NO3 Radicals and Implications for Gas- and Particle-Phase Reaction Mechanisms, J. Phys. Chem. A, 122(14), 3640–3652, doi:10.1021/acs.jpca.8b00692, 2018.

Craven, J. S., Yee, L. D., Ng, N. L., Canagaratna, M. R., Loza, C. L., Schilling, K. A., Yatavelli, R. L. N., Thornton, J. A., Ziemann, P. J., Flagan, R. C. and Seinfeld, J. H.: Analysis of secondary organic aerosol formation and aging using positive matrix factorization of high-resolution aerosol mass spectra: application to the dodecane low-NO_x system, Atmos. Chem. Phys., 12(24), 11795–11817, doi:10.5194/acp-12-11795-2012, 2012.

Day, D. A., Fry, J. L., Kang, H. G., Krechmer, J. E., Ayres, B. R., Keehan, N. I., Thompson, S. L., Hu, W., Campuzano-Jost, P., Schroder, J. C., Stark, H., DeVault, M. P., Ziemann, P. J., Zarzana, K. J., Wild, R. J., Dubè, W. P., Brown, S. S. and Jimenez, J. L.: Secondary Organic Aerosol Mass Yields from NO3 Oxidation of α-Pinene and Δ-Carene: Effect of RO2 Radical Fate, J. Phys. Chem. A, 126(40), 7309–7330, doi:10.1021/acs.jpca.2c04419, 2022.

DeCarlo, P. F., Slowik, J. G., Worsnop, D. R., Davidovits, P. and Jimenez, J. L.: Particle Morphology and Density Characterization by Combined Mobility and Aerodynamic Diameter Measurements. Part 1: Theory, Aerosol Sci. Technol., 38(12), 1185–1205, doi:10.1080/027868290903907, 2004.

DeCarlo, P. F., Kimmel, J. R., Trimborn, A., Northway, M. J., Jayne, J. T., Aiken, A. C., Gonin, M., Fuhrer, K., Horvath, T., Docherty, K. S., Worsnop, D. R. and Jimenez, J. L.: Field-deployable, high-resolution, time-of-flight aerosol mass spectrometer, Anal. Chem., 78(24), 8281–8289, doi:10.1021/ac061249n, 2006.

DeVault, M. P., Ziola, A. C. and Ziemann, P. J.: Products and Mechanisms of Secondary Organic Aerosol Formation from the NO3 Radical-Initiated Oxidation of Cyclic and Acyclic Monoterpenes, ACS Earth Space Chem., 6(8), 2076–2092, doi:10.1021/acsearthspacechem.2c00130, 2022.

Docherty, K. S., Jaoui, M., Corse, E., Jimenez, J. L., Offenberg, J. H., Lewandowski, M. and Kleindienst, T. E.: Collection Efficiency of the Aerosol Mass Spectrometer for Chamber-Generated Secondary Organic Aerosols, Aerosol Sci. Technol., 47(3), 294–309, doi:10.1080/02786826.2012.752572, 2013.

https://doi.org/10.5194/ar-2023-21
Preprint. Discussion started: 4 January 2024

Dockery, D. W., Cunningham, J., Damokosh, A. I., Neas, L. M., Spengler, J. D., Koutrakis, P., Ware, J. H., Raizenne, M. and Speizer, F. E.: Health effects of acid aerosols on North American children: respiratory symptoms, Environ. Health Perspect., 104(5), 500–505, doi:10.1289/ehp.96104500, 1996.

Dzepina, K., Arey, J., Marr, L. C., Worsnop, D. R., Salcedo, D., Zhang, Q., Onasch, T. B., Molina, L. T., Molina, M. J. and Jimenez, J. L.: Detection of particle-phase polycyclic aromatic hydrocarbons in Mexico City using an aerosol mass spectrometer, Int. J. Mass Spectrom., 263(2-3), 152–170, doi:10.1016/j.ijms.2007.01.010, 2007.

Eichler, P., Müller, M., D'Anna, B. and Wisthaler, A.: A novel inlet system for online chemical analysis of semi-volatile submicron particulate matter, Atmos. Meas. Tech., 8(3), 1353–1360, doi:10.5194/amt-8-1353-2015, 2015.

Farmer, D. K., Matsunaga, A., Docherty, K. S., Surratt, J. D., Seinfeld, J. H., Ziemann, P. J. and Jimenez, J. L.: Response of an aerosol mass spectrometer to organonitrates and organosulfates and implications for atmospheric chemistry, Proc. Natl. Acad. Sci. U. S. A., 107(15), 6670–6675, doi:10.1073/pnas.0912340107, 2010.

Gallimore, P. J. and Kalberer, M.: Characterizing an Extractive Electrospray Ionization (EESI) Source for the Online Mass Spectrometry Analysis of Organic Aerosols, Environ. Sci. Technol., 47(13), 7324–7331, doi:10.1021/es305199h, 2013.

Gao, Y., Walker, M. J., Barrett, J. A., Hosseinaei, O., Harper, D. P., Ford, P. C., Williams, B. J. and Foston, M. B.: Analysis of gas chromatography/mass spectrometry data for catalytic lignin depolymerization using positive matrix factorization, Green Chem., 20(18), 4366–4377, doi:10.1039/C8GC01474D, 2018.

Guo, H., Campuzano-Jost, P., Nault, B. A., Day, D. A., Schroder, J. C., Kim, D., Dibb, J. E., Dollner, M., Weinzierl, B. and Jimenez, J. L.: The importance of size ranges in aerosol instrument intercomparisons: a case study for the Atmospheric Tomography Mission, Atmos. Meas. Tech., 14(5), 3631–3655, doi:10.5194/amt-14-3631-2021, 2021.

IPCC: IPCC 2013: Climate Change 2013: The Physical Science Basis. Contribution of Working Group I to the Fifth Assessment Report of the Intergovernmental Panel on Climate Change, edited by T. F. Stocker, D. Qin, G. K. Plattner, M. Tignor, S. K. Allen, V. Bex, and P. M. Midgley, Cambridge University Press, Cambridge, United Kingdom and New York, NY, USA., 2013.

Jayne, J. T., Leard, D. C., Zhang, X., Davidovits, P., Smith, K. A., Kolb, C. E. and Worsnop, D. R.: Development of an Aerosol Mass Spectrometer for Size and Composition Analysis of Submicron Particles, Aerosol Sci. Technol., 33(1-2), 49–70, doi:10.1080/027868200410840, 2000.

Jimenez, J. L., Canagaratna, M. R., Donahue, N. M., Prevot, A. S. H., Zhang, Q., Kroll, J. H., DeCarlo, P. F., Allan, J. D., Coe, H., Ng, N. L., Aiken, A. C., Docherty, K. S., Ulbrich, I. M., Grieshop, A. P., Robinson, A. L., Duplissy, J., Smith, J. D., Wilson, K. R., Lanz, V. A., Hueglin, C., Sun, Y. L., Tian, J., Laaksonen, A., Raatikainen, T., Rautiainen, J., Vaattovaara, P., Ehn, M., Kulmala, M., Tomlinson, J. M., Collins, D. R., Cubison, M. J., Dunlea, E. J., Huffman, J. A., Onasch, T. B., Alfarra, M. R., Williams, P. I., Bower, K., Kondo, Y., Schneider, J., Drewnick, F., Borrmann, S., Weimer, S., Demerjian, K., Salcedo, D., Cottrell, L., Griffin, R., Takami, A., Miyoshi, T., Hatakeyama, S., Shimono, A., Sun, J. Y., Zhang, Y. M., Dzepina, K., Kimmel, J. R., Sueper, D., Jayne, J. T., Herndon, S. C., Trimborn, A. M., Williams, L. R., Wood, E. C., Middlebrook, A. M., Kolb, C. E., Baltensperger, U. and Worsnop, D. R.: Evolution of organic aerosols in the atmosphere, Science, 326(5959), 1525–1529, doi:10.1126/science.1180353, 2009.

Jimenez, J. L., Canagaratna, M. R., Drewnick, F., Allan, J. D., Alfarra, M. R., Middlebrook, A. M., Slowik, J. G., Zhang, Q., Coe, H., Jayne, J. T. and Worsnop, D. R.: Comment on "The effects of molecular weight and thermal decomposition on the sensitivity of a thermal desorption aerosol mass spectrometer," Aerosol Sci. Technol., 50(9), i–xv, doi:10.1080/02786826.2016.1205728, 2016.

Kanakidou, M., Seinfeld, J. H., Pandis, S. N., Barnes, I., Dentener, F. J., Facchini, M. C., Van Dingenen, R., Ervens, B., Nenes, A., Nielsen, C. J., Swietlicki, E., Putaud, J. P., Balkanski, Y., Fuzzi, S., Horth, J., Moortgat, G. K.,

https://doi.org/10.5194/ar-2023-21
Preprint. Discussion started: 4 January 2024

677 Winterhalter, R., Myhre, C. E. L., Tsigaridis, K., Vignati, E., Stephanou, E. G. and Wilson, J.: Organic aerosol and
678 global climate modelling: a review, Atmos. Chem. Phys., 5(4), 1053–1123, doi:10.5194/acp-5-1053-2005, 2005.

679 Kimmel, J. R., Farmer, D. K., Cubison, M. J., Sueper, D., Tanner, C., Nemitz, E., Worsnop, D. R., Gonin, M. and
680 Jimenez, J. L.: Real-time aerosol mass spectrometry with millisecond resolution, Int. J. Mass Spectrom., 303(1), 15–
681 26, doi:10.1016/j.ijms.2010.12.004, 2011.

682 Kruve, A., Kaupmees, K., Liigand, J. and Leito, I.: Negative electrospray ionization via deprotonation: predicting
683 the ionization efficiency, Anal. Chem., 86(10), 4822–4830, doi:10.1021/ac404066v, 2014.

684 Kumar, V., Giannoukos, S., Haslett, S. L., Tong, Y., Singh, A., Bertrand, A., Lee, C. P., Wang, D. S., Bhattu, D.,
685 Stefenelli, G., Dave, J. S., Puthussery, J. V., Qi, L., Vats, P., Rai, P., Casotto, R., Satish, R., Mishra, S., Pospisilova,
686 V., Mohr, C., Bell, D. M., Ganguly, D., Verma, V., Rastogi, N., Baltensperger, U., Tripathi, S. N., Prévôt, A. S. H.
687 and Slowik, J. G.: Highly time-resolved chemical speciation and source apportionment of organic aerosol
688 components in Delhi, India, using extractive electrospray ionization mass spectrometry, Atmos. Chem. Phys.,
689 22(11), 7739–7761, doi:10.5194/acp-22-7739-2022, 2022.

690 Kuwata, M., Zorn, S. R. and Martin, S. T.: Using elemental ratios to predict the density of organic material
691 composed of carbon, hydrogen, and oxygen, Environ. Sci. Technol., 46(2), 787–794, doi:10.1021/es202525q, 2012.

692 Lanz, V. A., Alfarra, M. R., Baltensperger, U., Buchmann, B., Hueglin, C. and Prévôt, A. S. H.: Source
693 apportionment of submicron organic aerosols at an urban site by factor analytical modelling of aerosol mass spectra,
694 Atmos. Chem. Phys., 7(6), 1503–1522, doi:10.5194/acp-7-1503-2007, 2007.

695 Law, W. S., Wang, R., Hu, B., Berchtold, C., Meier, L., Chen, H. and Zenobi, R.: On the mechanism of extractive
696 electrospray ionization, Anal. Chem., 82(11), 4494–4500, doi:10.1021/ac100390t, 2010.

697 Lee, E., Chan, C. K. and Paatero, P.: Application of positive matrix factorization in source apportionment of
698 particulate pollutants in Hong Kong, Atmos. Environ., 33(19), 3201–3212, doi:10.1016/S1352-2310(99)00113-2,
699 1999.

700 Lighty, J. S., Veranth, J. M. and Sarofim, A. F.: Combustion aerosols: factors governing their size and composition
701 and implications to human health, J. Air Waste Manag. Assoc., 50(9), 1565–618; discussion 1619–22 [online]
702 Available from: https://www.ncbi.nlm.nih.gov/pubmed/11055157, 2000.

703 Liigand, J., Wang, T., Kellogg, J., Smedsgaard, J., Cech, N. and Kruve, A.: Quantification for non-targeted LC/MS
704 screening without standard substances, Sci. Rep., 10(1), 5808, doi:10.1038/s41598-020-62573-z, 2020.

705 Liu, X., Day, D. A., Krechmer, J. E., Brown, W., Peng, Z., Ziemann, P. J. and Jimenez, J. L.: Direct measurements
706 of semi-volatile organic compound dynamics show near-unity mass accommodation coefficients for diverse
707 aerosols, Communications Chemistry, 2(1), 1–9, doi:10.1038/s42004-019-0200-x, 2019.

708 Lohmann, U., Broekhuizen, K., Leaitch, R., Shantz, N. and Abbatt, J.: How efficient is cloud droplet formation of
709 organic aerosols?, Geophys. Res. Lett., 31(5), 2004.

710 Lopez-Hilfiker, F. D., Mohr, C., Ehn, M., Rubach, F., Kleist, E., Wildt, J., Mentel, T. F., Lutz, A., Hallquist, M.,
711 Worsnop, D. and Thornton, J. A.: A novel method for online analysis of gas and particle composition: description
712 and evaluation of a Filter Inlet for Gases and AEROsols (FIGAERO), Atmos. Meas. Tech., 7(4), 983–1001,
713 doi:10.5194/amt-7-983-2014, 2014.

714 Lopez-Hilfiker, F. D., Pospisilova, V., Huang, W., Kalberer, M., Mohr, C., Stefenelli, G., Thornton, J. A.,
715 Baltensperger, U., Prevot, A. S. H. and Slowik, J. G.: An extractive electrospray ionization time-of-flight mass
716 spectrometer for online measurement of atmospheric particles, Atmos. Meas. Tech., 12(9), 4867–4886,
717 doi:10.5194/amt-12-4867-2019, 2019.

https://doi.org/10.5194/ar-2023-21
Preprint. Discussion started: 4 January 2024

718 Nault, B. A., Campuzano-Jost, P., Day, D. A., Schroder, J. C., Anderson, B., Beyersdorf, A. J., Blake, D. R., Brune,
719 W. H., Choi, Y., Corr, C. A., Gouw, J. A. de, Dibb, J., DiGangi, J. P., Diskin, G. S., Fried, A., Huey, L. G., Kim, M.
720 J., Knote, C. J., Lamb, K. D., Lee, T., Park, T., Pusede, S. E., Scheuer, E., Thornhill, K. L., Woo, J.-H. and Jimenez,
721 J. L.: Secondary organic aerosol production from local emissions dominates the organic aerosol budget over Seoul,
722 South Korea, during KORUS-AQ, Atmos. Chem. Phys., 18(24), 17769–17800, doi:10.5194/acp-18-17769-2018,
723 2018.

724 Nault, B. A., Croteau, P., Jayne, J., Williams, A., Williams, L., Worsnop, D., Katz, E. F., DeCarlo, P. F. and
725 Canagaratna, M.: Laboratory evaluation of organic aerosol relative ionization efficiencies in the aerodyne aerosol
726 mass spectrometer and aerosol chemical speciation monitor, Aerosol Sci. Technol., 1–17,
727 doi:10.1080/02786826.2023.2223249, 2023.

728 Paatero, P.: Least squares formulation of robust non-negative factor analysis, Chemometrics Intellig. Lab. Syst.,
729 37(1), 23–35, doi:10.1016/S0169-7439(96)00044-5, 1997.

730 Paatero, P.: The Multilinear Engine: A Table-Driven, Least Squares Program for Solving Multilinear Problems,
731 including the n-Way Parallel Factor Analysis Model, J. Comput. Graph. Stat., 8(4), 854–854, doi:10.2307/1390831,
732 1999.

733 Paatero, P.: End user's guide to multilinear engine applications, University of Helsinki, Helsinki, Finland., 2007.

734 Paatero, P. and Tapper, U.: Positive Matrix Factorization - A Nonnegative Factor Model With Optimal Utilization of
735 Error-Estimates of Data Values, Environmetrics, 5(2), 111–126, 1994.

736 Pagonis, D., Campuzano-Jost, P., Guo, H., Day, D. A., Schueneman, M. K., Brown, W. L., Nault, B. A., Stark, H.,
737 Siemens, K., Laskin, A., Piel, F., Tomsche, L., Wisthaler, A., Coggon, M. M., Gkatzelis, G. I., Halliday, H. S.,
738 Krechmer, J. E., Moore, R. H., Thomson, D. S., Warneke, C., Wiggins, E. B. and Jimenez, J. L.: Airborne extractive
739 electrospray mass spectrometry measurements of the chemical composition of organic aerosol, Atmospheric
740 Measurement Techniques, 14(2), 1545–1559, doi:10.5194/amt-14-1545-2021, 2021.

741 Pospisilova, V., Lopez-Hilfiker, F. D., Bell, D. M., El Haddad, I., Mohr, C., Huang, W., Heikkinen, L., Xiao, M.,
742 Dommen, J., Prevot, A. S. H., Baltensperger, U. and Slowik, J. G.: On the fate of oxygenated organic molecules in
743 atmospheric aerosol particles, Science Advances, 6(11), eaax8922, doi:10.1126/sciadv.aax8922, 2020.

744 Qi, L., Chen, M., Stefenelli, G., Pospisilova, V., Tong, Y., Bertrand, A., Hueglin, C., Ge, X., Baltensperger, U.,
745 Prévôt, A. S. H. and Slowik, J. G.: Organic aerosol source apportionment in Zurich using an extractive electrospray
746 ionization time-of-flight mass spectrometer (EESI-TOF-MS) – Part 2: Biomass burning influences in winter, Atmos.
747 Chem. Phys., 19(12), 8037–8062, doi:10.5194/acp-19-8037-2019, 2019.

748 Qi, L., Vogel, A. L., Esmaeilirad, S., Cao, L., Zheng, J., Jaffrezo, J.-L., Fermo, P., Kasper-Giebl, A., Daellenbach,
749 K. R., Chen, M., Ge, X., Baltensperger, U., Prévôt, A. S. H. and Slowik, J. G.: A 1-year characterization of organic
750 aerosol composition and sources using an extractive electrospray ionization time-of-flight mass spectrometer (EESI-
751 TOF), Atmospheric Chemistry and Physics, 20(13), 7875–7893, doi:10.5194/acp-20-7875-2020, 2020.

752 Slowik, J. G., Stainken, K., Davidovits, P., Williams, L. R., Jayne, J. T., Kolb, C. E., Worsnop, D. R., Rudich, Y.,
753 DeCarlo, P. F. and Jimenez, J. L.: Particle Morphology and Density Characterization by Combined Mobility and
754 Aerodynamic Diameter Measurements. Part 2: Application to Combustion-Generated Soot Aerosols as a Function of
755 Fuel Equivalence Ratio, Aerosol Sci. Technol., 38(12), 1206–1222, doi:10.1080/027868290903916, 2004.

756 Stefenelli, G., Pospisilova, V., Lopez-Hilfiker, F. D., Daellenbach, K. R., Hüglin, C., Tong, Y., Baltensperger, U.,
757 Prévôt, A. S. H. and Slowik, J. G.: Organic aerosol source apportionment in Zurich using an extractive electrospray
758 ionization time-of-flight mass spectrometer (EESI-TOF-MS)--Part 1: Biogenic influences and day--night chemistry
759 in summer, Atmos. Chem. Phys., 19(23), 14825–14848 [online] Available from:
760 https://acp.copernicus.org/articles/19/14825/2019/, 2019.

https://doi.org/10.5194/ar-2023-21
Preprint. Discussion started: 4 January 2024

Sueper, D.: ToF-AMS Data Analysis Software Webpage, [online] Available from: http://cires1.colorado.edu/jimenez-group/wiki/index.php/ ToF-AMS_Analysis_Software (Accessed 13 April 2023), 2023.

Takeuchi, M., Wang, Y., Nault, B. A., Canagaratna, M. and Ng, N. L.: Potential Underestimation of Particulate Organic Nitrate Concentration by an Aerosol Mass Spectrometer, [online] Available from: https://aaarabstracts.com/2021/viewabstract.php?pid=221, October 18-22 2021.

Tennison, S. R.: Phenolic-resin-derived activated carbons, Appl. Catal. A, 173(2), 289–311, doi:10.1016/S0926-860X(98)00186-0, 1998.

Tong, Y., Qi, L., Stefenelli, G., Wang, D. S., Canonaco, F., Baltensperger, U., Prévôt, A. S. H. and Slowik, J. G.: Quantification of primary and secondary organic aerosol sources by combined factor analysis of extractive electrospray ionisation and aerosol mass spectrometer measurements (EESI-TOF and AMS), Atmospheric Measurement Techniques, 15(24), 7265–7291, doi:10.5194/amt-15-7265-2022, 2022.

Ulbrich, I. M., Canagaratna, M. R., Zhang, Q., Worsnop, D. R. and Jimenez, J. L.: Interpretation of organic components from positive matrix factorization of aerosol mass spectrometric data, Atmospheric Chemistry & Physics, 9(9) [online] Available from: https://d-nb.info/114970523X/34, 2009.

Ulbrich, I. M., Handschy, A. V., Lechner, M. and Jimenez, J. L.: High-Resolution AMS Spectral Database, [online] Available from: http://cires.colorado.edu/jimenez-group/HRAMSsd/, 2019.

Wang, D. S., Lee, C. P., Krechmer, J. E., Majluf, F., Tong, Y., Canagaratna, M. R., Schmale, J., Prévôt, A. S. H., Baltensperger, U., Dommen, J., El Haddad, I., Slowik, J. G. and Bell, D. M.: Constraining the response factors of an extractive electrospray ionization mass spectrometer for near-molecular aerosol speciation, Atmos. Meas. Tech., 14(11), 6955–6972, doi:10.5194/amt-14-6955-2021, 2021.

Xu, W., Lambe, A., Silva, P., Hu, W., Onasch, T., Williams, L., Croteau, P., Zhang, X., Renbaum-Wolff, L., Fortner, E., Jimenez, J. L., Jayne, J., Worsnop, D. and Canagaratna, M.: Laboratory evaluation of species-dependent relative ionization efficiencies in the Aerodyne Aerosol Mass Spectrometer, Aerosol Sci. Technol., 52(6), 626–641, doi:10.1080/02786826.2018.1439570, 2018.

Zhang, Q., Alfarra, M. R., Worsnop, D. R., Allan, J. D., Coe, H., Canagaratna, M. R. and Jimenez, J. L.: Deconvolution and quantification of hydrocarbon-like and oxygenated organic aerosols based on aerosol mass spectrometry, Environ. Sci. Technol., 39(13), 4938–4952, doi:10.1021/es048568l, 2005.

Zhang, Q., Jimenez, J. L., Canagaratna, M. R., Allan, J. D., Coe, H., Ulbrich, I., Alfarra, M. R., Takami, A., Middlebrook, A. M., Sun, Y. L., Dzepina, K., Dunlea, E., Docherty, K., DeCarlo, P. F., Salcedo, D., Onasch, T., Jayne, J. T., Miyoshi, T., Shimono, A., Hatakeyama, S., Takegawa, N., Kondo, Y., Schneider, J., Drewnick, F., Borrmann, S., Weimer, S., Demerjian, K., Williams, P., Bower, K., Bahreini, R., Cottrell, L., Griffin, R. J., Rautiainen, J., Sun, J. Y., Zhang, Y. M. and Worsnop, D. R.: Ubiquity and dominance of oxygenated species in organic aerosols in anthropogenically-influenced Northern Hemisphere midlatitudes, Geophys. Res. Lett., 34(13), doi:10.1029/2007gl029979, 2007.

Zhang, Y., Williams, B. J., Goldstein, A. H., Docherty, K., Ulbrich, I. M. and Jimenez, J. L.: A Technique for Rapid Gas Chromatography Analysis Applied to Ambient Organic Aerosol Measurements from the Thermal Desorption Aerosol Gas Chromatograph (TAG), Aerosol Sci. Technol., 48(11), 1166–1182, doi:10.1080/02786826.2014.967832, 2014.

Zhang, Y., Williams, B. J., Goldstein, A. H., Docherty, K. S. and Jimenez, J. L.: A technique for rapid source apportionment applied to ambient organic aerosol measurements from a thermal desorption aerosol gas chromatograph (TAG), Atmospheric Measurement Techniques, 9(11), 5637–5653, doi:10.5194/amt-9-5637-2016, 2016.